Energy-band-structure studies of NbN(100) and VN(100)

A. Callenås and L. I. Johansson
Department of Physics and Measurement Technology, Linköping University, S-581 83 Linköping, Sweden

A. N. Christensen
Department of Chemistry, Aarhus University, DK-8000 Aarhus C, Denmark

K. Schwarz and P. Blaha
Institute of Technical Electrochemistry, Technical University of Vienna, A-1060, Vienna, Austria
(Received 31 January 1985)

Band-structure studies of NbN and VN are reported. The results of angle-resolved photoemission experiments performed on $NbN_{0.93}$ and $VN_{0.89}$ are presented. The bulk-band structures calculated for stoichiometric NbN and VN using the linearized augmented-plane-wave method are presented and utilized in the interpretation of the experimental spectra. It is shown that most of the features in the spectra can be accounted for by direct bulk-band transitions. A fairly good agreement between experimental and calculated band locations and dispersions is obtained.

I. INTRODUCTION

The transition-metal nitrides and carbides form an interesting class of materials since they show an unusual combination of physical and electrical properties.[1] These properties, such as extremely high melting points, extreme hardness, and metallic conductivity, are related to their electronic structure. Detailed studies of the electronic structure of these materials seem therefore well motivated. Such studies have earlier been reported on TiC,[2,3] TiN,[4] and ZrN,[5] and in this paper a detailed study of NbN and VN is presented. The results of angle-resolved photoemission experiments and of band-structure calculations on NbN and VN are reported. Earlier angle-integrated photoemission experiments on NbN (Ref. 6) and VN (Ref. 7) provided information only about the total density of occupied states.

Together with angle-resolved photoemission results on NbN(100) and VN(100), band-structure calculations carried out for stoichiometric $NbN_{1.0}$ and $VN_{1.0}$ using the linear augmented-plane-wave (LAPW) method are reported. The calculated band structures are used together with the direct-transition model to interpret the experimental results. This method of interpretation in terms of direct bulk-band transitions has earlier been shown to work well[3–5] for (100) surfaces of other transition-metal nitrides and carbides. Also, for VN(100) and NbN(100) it is shown below that most of the structures in the photoemission spectra can be interpreted as originating from direct transitions between bulk bands. In contrast to the results obtained on some other nitrides,[8] no surface-induced feature was observed on NbN(100) and VN(100).

II. EXPERIMENTAL

A single crystal of cubic δ-NbN was made by annealing a single crystal of tetragonal γ-NbN in pure nitrogen. The single crystal of γ-NbN was made by annealing a polycrystalline rode of niobium of 99.99% purity in a nitrogen atmosphere of nominal 99.99% purity at a pressure of 2 MPa. The annealing temperature was approximately 2100 °C, and the annealing time 100 h. The annealing of γ-NbN to δ-NbN was made at the same nitrogen pressure at 2300 °C for 150 h. The lattice constant for the cubic δ-NbN crystal was determined from a Guinier powder pattern using Cu $K\alpha$ radiation and silicon as an internal standard. The composition of the crystal was determined from the variation of the cell constant with the composition ratio x in NbN_x,[9,10] and also gravimetrically by ignition of NbN in air at 1100 °C to Nb_2O_5. The two measurements agreed with each other and yielded the composition $NbN_{0.93}$.

The vanadium nitride crystal was made by zone-melting crystal growth of a polycrystalline rod of VN with an almost stoichiometric composition.[11] Guinier photographs were taken of the single crystal using the same procedure as described above, and form the variation of the cubic-unit-cell parameter with the ratio x in VN_x the composition of the single crystal was determined to be $VN_{0.74}$.[12] The crystal was annealed in 99.99% pure nitrogen at 1.85 MPa and 1950 °C for approximately 150 h. After this treatment the composition was found to be $VN_{0.89}$. Both NbN and VN crystallize in the rocksalt structure.

The conventional angle-resolved photoemission system used in these experiments was described earlier.[4] High-temperature flashings were used in order to achieve a clean VN(100) surface. Flashings to about 1100 °C were found to produce a clean surface. The NbN(100) surface was cleaned by sputtering with argon ions followed by annealings to about 800 °C. The cleanliness of the samples was checked with Auger electron spectroscopy. The crystals were exposed to CO and O_2 at room temperature using pressures in the 10^{-7}–10^{-5}-Pa range, in order to check if any feature in the spectra was particularly sensitive to surface contamination.

Both crystals were oriented azimuthally prior to mounting in the spectrometer with the aid of x-ray diffraction. In the spectra shown below, the incidence angle of the radiation, θ_i, and the electron-emission angle, θ_e, are given relative to the sample surface normal. The midpoint of the Fermi edge is used as the reference level in all spectra.

III. RESULTS AND DISCUSSION

A. Band-structure calculations

An interpretation of the photoelectron spectra by direct transitions between bulk bands has worked in similar cases.[3–5] Before describing how the energy bands are calculated in the present case, two remarks should be made: (i) in connection with TiC it has been discussed[3] that the eigenvalues $\epsilon(n,k)$ are not rigorously the system's excitation energies; (ii) the real crystal is not stoichiometric, so that even for bulk properties (neglecting the surface) the assumed NaCl structure is an idealization.

The energy bands of the two compounds studied here have both been calculated using the self-consistent augmented-plane-wave (APW) method, where the effects of exchange and correlation are approximated by the $X\alpha$ method; this was done by Schwarz[13,14] for NbN and by Neckel *et al.*[15] for VN.

For the present analysis we need band energies on a fine **k** grid up to about 40 eV above the Fermi level. These energies should approximate the final state of the photoelectron process. Since such data are not available from the earlier publications of Schwarz and co-workers,[13,15] we use their self-consistent APW potentials and perform new calculations by the linearized APW method (LAPW).[16] The energies were calculated for a plane through the Brillouin zone surrounded by the **k** points Γ-(Δ)-*X*-*U*-*L*-*K*-(Σ)-Γ. In this plane a uniform mesh of 149 **k** points is obtained by dividing the Δ direction into 16 and the Σ direction into 12 intervals. The LAPW calculation for VN is done nonrelativistically as was the work on TiN.[4] Since it was found[5] that in ZrN relativistic effects are no longer negligible, they were approximately taken into account by the technique of Koelling and Harmon,[17] in which the Dirac equation is solved by dropping the spin-orbit interaction. Consequently the same pseudorelativistic LAPW calculation (as for ZrN) is chosen for NbN. Since the energy dependence of the radial wave functions can be linearized over an energy range of about 12 eV, in both cases four energy sheets were required to span the whole energy range of interest. In every sheet the wave functions are expanded around E_l (for definitions see Ref. 16) and the same parameters E_l are taken for VN as for TiN,[4] and for NbN as for ZrN.[5] Although for both compounds the LAPW calculations were done with an unsymmetrized version, the symmetry labels of the energy eigenvalues can be obtained by applying projection operators afterwards. These LAPW results together with compatibility relations yield the complete band structures shown in Figs. 1 and 2.

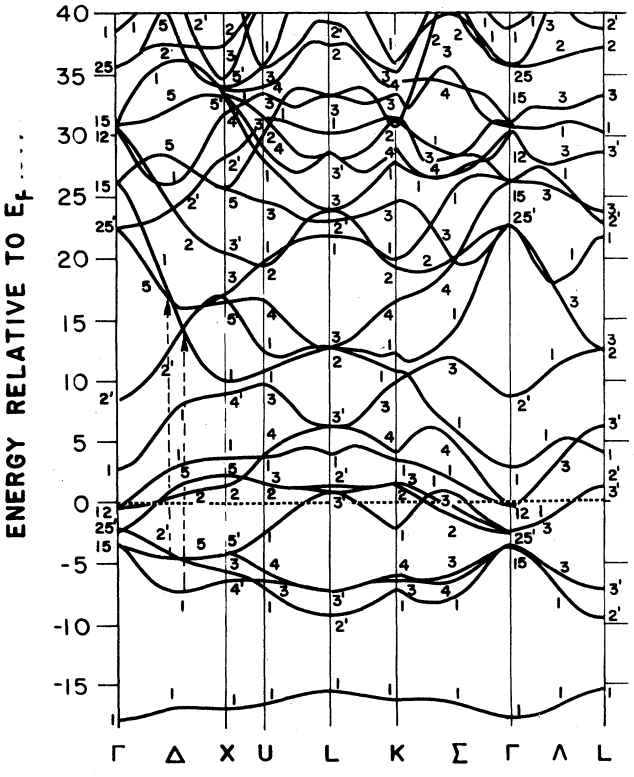

FIG. 1. Energy bands of NbN calculated by the pseudorelativistic LAPW method. The dashed arrows illustrate direct transitions using He I radiation (peaks *B* and *D* in Fig. 3).

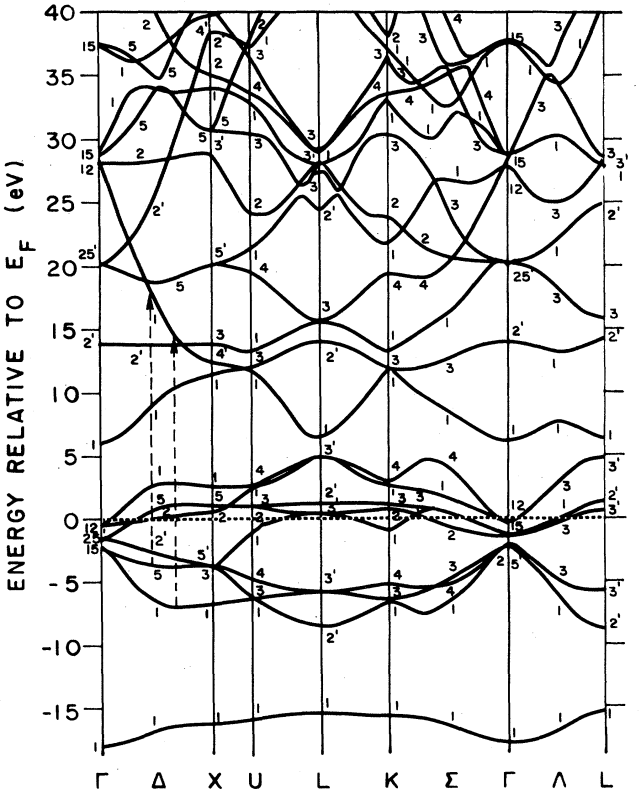

FIG. 2. Calculated energy bands of VN using the LAPW method. Direct transitions for He I radiation are illustrated by the dashed arrows (peaks *A* and *B* in Fig. 7).

B. NbN(100)

In Fig. 3 angle-resolved electron-energy distribution curves (EDC's) recorded from the NbN(100) surface using unpolarized He I (21.2 eV) radiation are shown. The spectra were recorded at different polar angles, θ_e, along the $\langle 011 \rangle$ azimuth thus probing the Γ-(Δ)-X-U-L-K-(Σ)-Γ plane of the bulk Brillouin zone. In order to identify the symmetry of the initial states, spectra were recorded at two different incidence angles, θ_i, of the light. In Fig. 3(a) the incidence angle is 15° and in Fig. 3(b) it is 45°. Symmetry-selection rules[18] show, for normal electron emission, $\theta_e = 0°$, that the electric field component parallel to the surface, $E_{\|}$, excites only initial states of Δ_5 symmetry while the perpendicular component $E_{\perp}$ excites only initial states of Δ_1 symmetry. Since $E_{\|}/E_{\perp}$ is greater for $\theta_i = 15°$ than for $\theta_i = 45°$ the symmetry of the initial states can be identified. The normal-emission spectra in Figs. 3(a) and 3(b) show that peak B should be associated with emission from a Δ_5 initial-state band and that peaks C and D can be identified as arising from initial states of Δ_1 symmetry.

By using the band-structure results (Fig. 1) and the direct-transition model, peak B can be interpreted as arising from transitions between the initial-state band of Δ_5 symmetry at about 4.4 eV below the Fermi level and the final-state band of Δ_1 symmetry at about 16.8 eV above the Fermi level, Δ_5 ($E_F - 4.4$ eV)$\rightarrow\Delta_1$ ($E_F + 16.8$ eV) (see dashed arrow along the $\Gamma \rightarrow X$ symmetry line in Fig. 1).

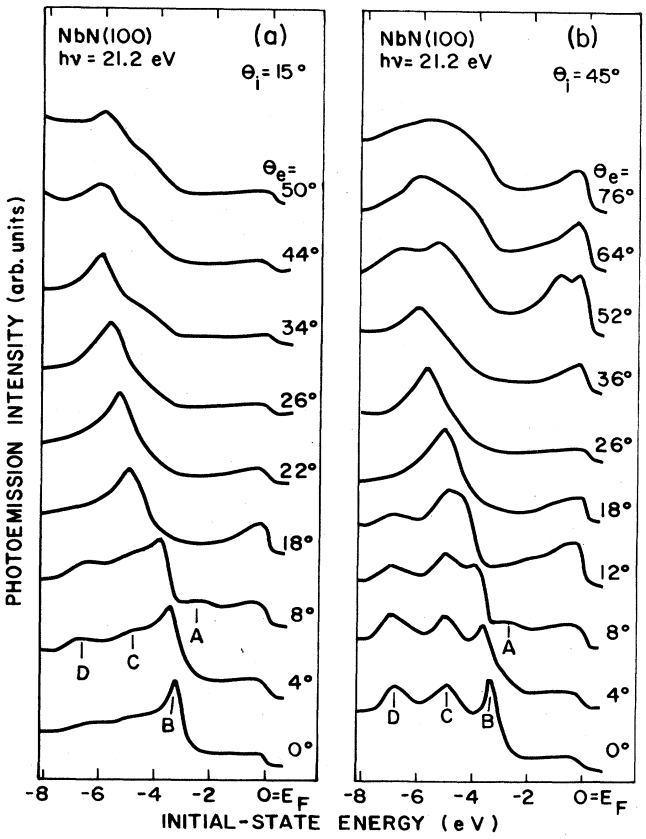

FIG. 3. Angle-resolved He I spectra from NbN(100) measured at various polar angles θ_e.

Peak D, at about -6.9 eV in Fig. 3(b), corresponds to transitions between the initial-state band of Δ_1 symmetry at -7.3 eV and the final-state band of Δ_1 symmetry at 13.9 eV above the Fermi level, Δ_1 ($E_F - 7.3$ eV)$\rightarrow\Delta_1$ ($E_F + 13.9$ eV) (see dashed arrow in Fig. 1).

The peak labeled A in Fig. 3 we attribute to emission from the initial state band of $\Delta_{2'}$ symmetry. This peak only appears in the off-normal spectra, as it should according to symmetry-selection rules.

The polarization dependence observed for the peak labeled C, at about -5.0 eV, associates this peak with transitions from an initial state of Δ_1 symmetry. However, when using the direct-transition model and the band-structure calculation shown in Fig. 1, there is no corresponding Δ_1 initial state available. Therefore we believe that density-of-state (DOS) effects may give rise to this structure, and since it exhibits Δ_1 symmetry it may reflect the location of the relatively flat portion of the Δ_1 band extending around the $X_{4'}$ point. A similar structure is also observed in the spectra recorded using Ne I (16.85 eV) radiation as discussed below.

In the photoemission process the component of momentum parallel to the surface, $\bar{k}_{\|}$, and the energy are conserved. By measuring the kinetic energy and the emission direction outside the crystal, the initial-state energy $E_i(k_{\|})$ of the photoexcited electron inside the crystal can be determined. The momentum component parallel to the surface is

$$|k_{\|}| = \frac{[2m(h\nu + E_i - \phi)]^{1/2}}{\hbar} \sin\theta_e ,$$

where E_i represents the initial-state energy, θ_e the polar angle, and ϕ the work function. In the calculation of $k_{\|}$ a work function of 3.8 eV was used. This value was determined from the low-energy cutoff in the photoemission spectra. In Fig. 4 the measured and calcuated $E_i(k_{\|})$ are compared. The dots correspond to the experimentally determined locations of peaks A, B, C, and D and the dashed lines to the calculated dispersions. The calculated results were obtained from the full band structure using the same method as in a previous paper.[4] Both primary-cone emission and secondary-cone emission, involving a $G_{\bar{1}\bar{1}\bar{1}}$ reciprocal-lattice vector, were included in the calculation. When comparing experimental and calculated results in Fig. 4 a good agreement is obtained for peaks A and D. Peak B is seen to lie about 1.0 eV closer to the Fermi level than the calculated position at $\theta_e = 0°$, but the dispersion of this peak agrees well with the calculated dispersion. There is no calculated band dispersion that fits with the dispersion determined for peak C.

Measurements using unpolarized Ne I radiation (16.85 eV) were also performed on the NbN(100) surface as shown in Fig. 5. These spectra were recorded at different polar angles along the same azimuth as the He I spectra shown in Fig. 3. Three peaks, labeled B, C, and D, are clearly seen in Fig. 5. According to the above-mentioned symmetry-selection rules, peak B, at about -3.4 eV, can be interpreted as due to transitions from a Δ_5 initial-state band, thus reflecting transitions Δ_5 ($E_F - 4.2$ eV)$\rightarrow\Delta_1$

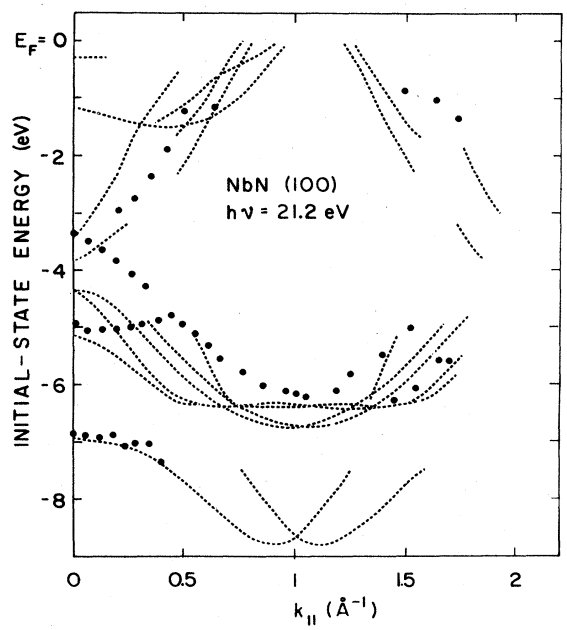

FIG. 4. Comparison between experimental and calculated peak positions as functions of $k_{\parallel}$, along the ⟨011⟩ azimuth. See text for details.

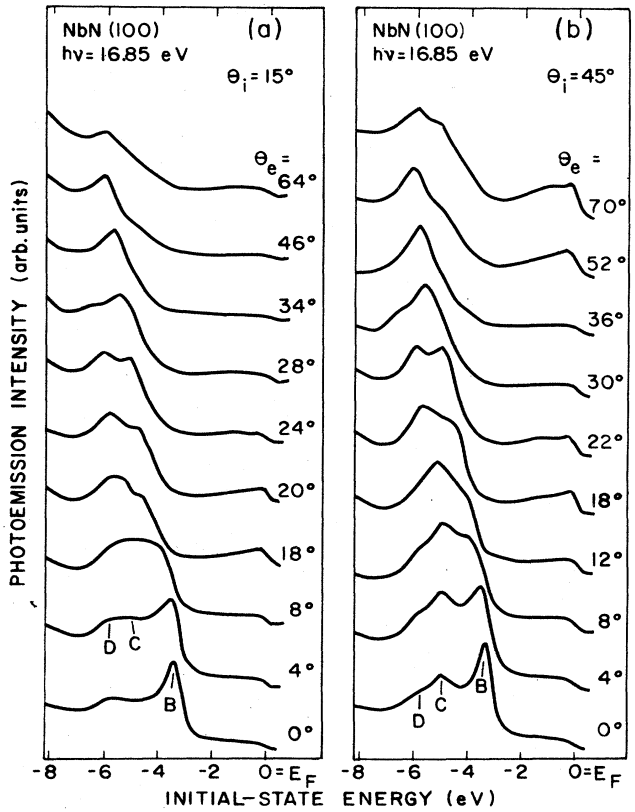

FIG. 5. Angle-resolved NeI spectra from NbN(100) measured at various polar angles θ_e.

($E_F+12.6$ eV) in the calculated band structure. Transitions between the Δ_1 initial-state band and the Δ_1 final-state band, Δ_1 ($E_F-6.3$ eV)$\rightarrow\Delta_1(E_F+10.5$ eV), can likewise explain the origin of peak D in Fig. 5. The experimental position of this peak is at an initial-state energy of about -5.8 eV in the normal emission spectrum, see Fig. 5(a). The peak at -5.0 eV, labeled C in Fig. 5(b), is interpreted as due to DOS effects as discussed above for the peak C in Fig. 3. In this case peak C is observed to disperse toward lower initial-state energy as the polar angle increases above 10°.

In Fig. 6 the energy positions of the peaks shown in Fig. 5 are plotted versus $k_{\parallel}$ (dots) and the calculated dispersions are shown as dashed lines. Also, at this photon energy the trends in the experimental peak positions agree fairly well with the trends of the calculated value. However, the experimental value of peak B, at $\theta_e=0°$, lies about 0.8 eV closer to the Fermi level than the calculated value. Since peak C in Fig. 5 is believed to be due to DOS effects there should be no calculated band in Fig. 6 corresponding to this peak. In order to see if this peak may reflect the flat portion of the Δ_1 band around the $X_{4'}$ point the dispersion of this part of the band structure was calculated and is shown as a solid line in Fig. 6. If this line is shifted 1 eV towards the Fermi level it falls right on top of the experimentally determined energy positions of peak C (also valid in Fig. 4). This lends support ot our interpretation of peak C and it suggests that the $X_{4'}$ point in the band-structure calculation should be moved 1 eV closer to the Fermi level.

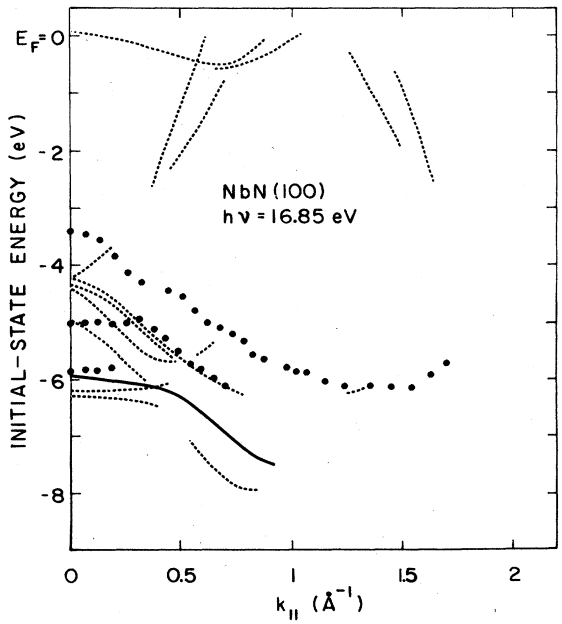

FIG. 6. Comparison between experimental and calculated peak positions as functions of $k_{\parallel}$, along the ⟨011⟩ azimuth. The solid line represents the calculated dispersion of the $X_{4'}$ point.

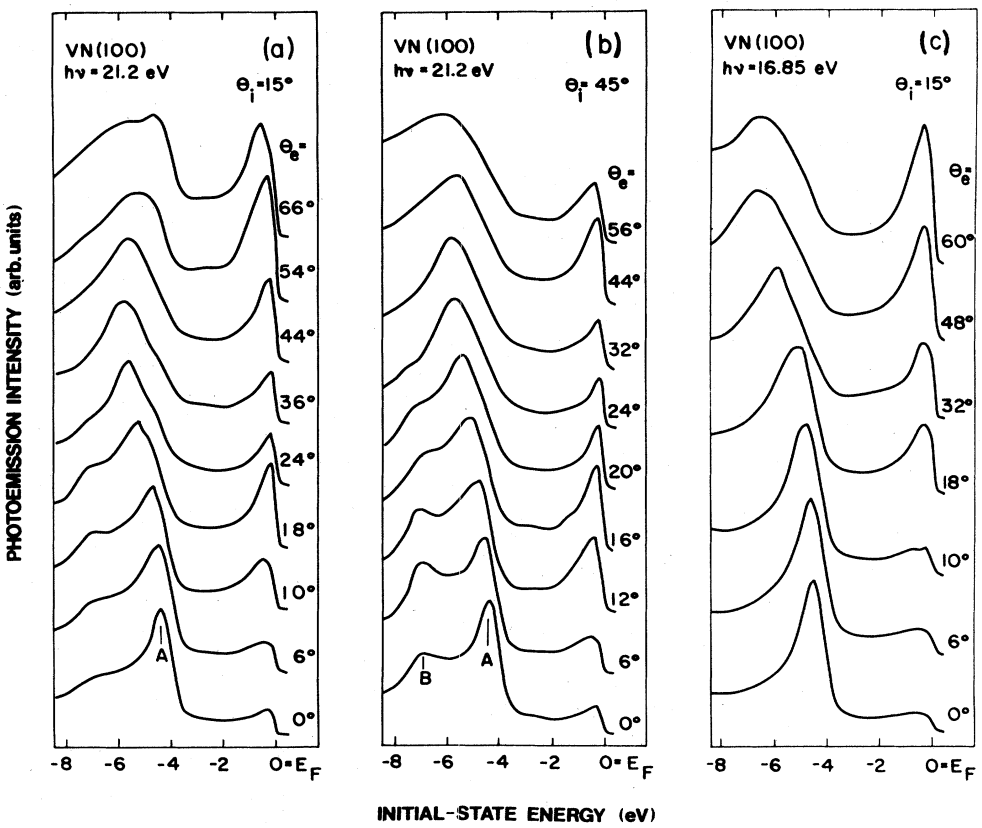

FIG. 7. (a) and (b) angle-resolved He I and (c) Ne I spectra from VN(100) measured at various polar angles θ_e.

C. VN(100)

Angle-resolved EDC's from VN(100) recorded at different polar angles, θ_e, along the $\langle 011 \rangle$ azimuth using unpolarized He I (21.2 eV) and Ne I (16.85 eV) radiation are shown in Fig. 7. The normal emission He I spectra in Figs. 7(a) and 7(b) show two prominent peaks labeled A and B. These peaks can easily be identified by using the band-structure calculation, the direct-transition model, and symmetry-selection rules. Peak B, at about -6.9 eV initial-state energy, is best seen in Fig. 7(b) where an incidence angle θ_i of 45° was used. Transitions between the Δ_1 initial-state band and the Δ_1 final-state band, Δ_1 ($E_F-6.8$ eV)$\rightarrow\Delta_1$ ($E_F+14.4$ eV), give rise to this peak (see dashed arrow in Fig. 2). The peak at about -4.4 eV, labeled A in Fig. 7, is due to transitions from the Δ_5 initial-state band to the Δ_1 final-state band, Δ_5 ($E_F-3.6$ eV)$\rightarrow\Delta_1$ ($E_F+17.6$ eV). (Illustrated as a dashed arrow in Fig. 2). A dispersion towards lower initial-state energy is observed for this peak as the polar angle increases.

The energy positions of peaks A and B are in Fig. 8 plotted versus $k_{||}$ (dots). Also shown in this figure are dots corresponding to the peak at the Fermi level. This peak appears in the off-normal emission spectra and is quite strong at emission angles θ_e, between 10° and 20° and at $\theta_e > 40°$, as seen in Fig. 7. The calculated band dispersions using the full band structure, and a work function of 3.9 eV, are shown in Fig. 8 as dashed lines. A fairly good agreement between experimental and calculated results is obtained as seen in Fig. 8. For peak A, however, the calculated energy position is about 0.9 eV closer to the Fermi level than the experimental value at normal emission.

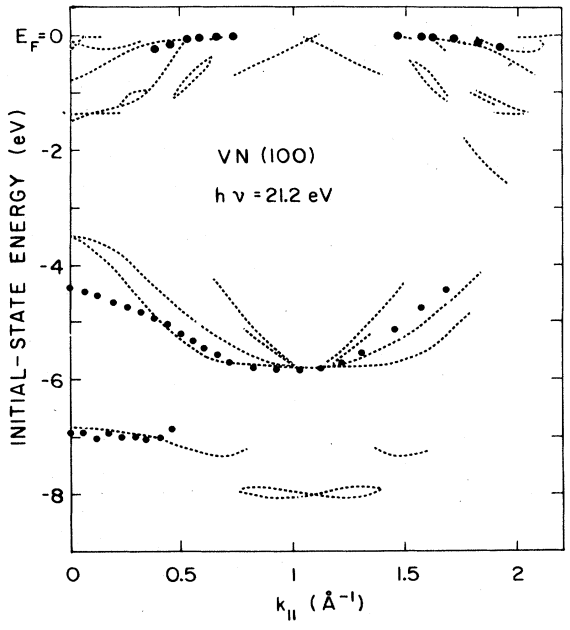

FIG. 8. Comparison between experimental and calculated peak positions as functions of $k_{||}$, along the $\langle 011 \rangle$ azimuth.

In Fig. 7(c) EDC's recorded using a photon energy of 16.85 eV and an incidence angle of 15° are shown. A single dominant peak is observed at about -4.6 eV in the normal emission spectrum. Symmetry selection rules can again be used which show that transitions between the Δ_5 initial-state band and the Δ_1 final-state band, Δ_5 $(E_F-3.6\text{ eV})\rightarrow\Delta_1$ $(E_F+13.3\text{ eV})$, do account for this dominant peak. The dispersion determined for this structure and the calculated dispersion using the full band structure give results very similar to the ones shown in Fig. 8 and are therefore not shown.

IV. SUMMARY

The angle-resolved photoemission technique has been used to study the electronic structure of NbN and VN in detail. Experiments were carried out on the (100) surface of the nonstoichiometric single crystals $NbN_{0.93}$ and $VN_{0.89}$. The bulk band structure of stoichiometric NbN and VN was calculated using the linearized augmented-plane-wave method (LAPW) and was utilized in the interpretation of the experimental data.

Most of the structures observed from the NbN(100) and the VN(100) surfaces could be explained in terms of direct transitions between bulk energy bands. This method allowed direct identification of individual bands, whose energy locations and dispersions could be mapped out and a fairly good agreement between experimental and calculated results were obtained. On the NbN(100) surface, however, there was one structure that could not be interpreted as arising from direct bulk-band transitions. This structure, labeled *C* in Figs. 3 and 5, was interpreted as reflecting DOS effects. Apart from this structure the agreement between calculated and experimental results for NbN(100) and VN(100) was as good as that demonstrated earlier for TiC(100),[3] TiN(100),[4] and ZrN(100).[5]

[1]L. E. Toth, *Transition Metal Carbides and Nitrides* (Academic, New York, 1971).
[2]J. H. Weaver, A. M. Bradshaw, J. F. van der Veen, F. J. Himpsel, D. E. Eastman, and C. Politis, Phys. Rev. B **22**, 4921 (1980).
[3]A. Callenås, L. I. Johansson, A. N. Christensen, K. Schwarz, and J. Redinger, Phys. Rev. B **27**, 5934 (1983).
[4]L. I. Johansson, A. Callenås, P. M. Stefan, A. N. Christensen, and K. Schwarz, Phys. Rev. B **24**, 1883 (1981).
[5]A. Callenås, L. I. Johansson, A. N. Christensen, K. Schwarz, P. Blaha, and J. Redinger, Phys. Rev. B **30**, 635 (1984).
[6]W. K. Schubert, R. N. Shelton, and E. L. Wolf, Phys. Rev. B **24**, 6278 (1981).
[7]W. K. Schubert, R. N. Shelton, and E. L. Wolf, Phys. Rev. B **23**, 5097 (1981).
[8]A. Callenås and L. I. Johansson, Solid State Commun. **52**, 143 (1984).
[9]K. E. Storms, High Temp. Sci. **7**, 103 (1975).
[10]R. Kaiser, W. Spengler, S. Schicktanz, and C. Politis, Phys. Status Solidi B **87**, 565 (1978).
[11]A. N. Christensen and P. Roedhammer, J. Cryst. Growth **38**, 281 (1977).
[12]G. Braver and W. D. Schnell, J. Less-Common Met. **6**, 326 (1964).
[13]K. Schwarz, Monatsh. Chem. **102**, 1400 (1971).
[14]K. Schwarz, J. Phys. C **8**, 809 (1975); **10**, 195 (1977).
[15]A. Neckel, P. Rastl, R. Eibler, P. Weinberger, and K. Schwarz, J. Phys. C **9**, 579 (1976).
[16]O. K. Andersen, Phys. Rev. B **12**, 3060 (1976); D. D. Koelling and G. O. Arbman, J. Phys. C **5**, 2041 (1975).
[17]D. D. Koelling and B. N. Harmon, J. Phys. C **10**, 3107 (1977).
[18]J. Hermanson, Solid State Commun. **22**, 9 (1977).